JOURNAL OF GEOPHYSICAL RESEARCH, VOL. 105, NO. C12, PAGES 28,527–28,546, DECEMBER 15, 2000

Flow through Denmark Strait

Rolf. H. Käse and Andreas Oschlies
Institut für Meereskunde an der Universität Kiel, Kiel, Germany

Abstract. On the basis of hydrographic observations taken in the vicinity of Denmark Strait, a primitive equation model is used to investigate physical mechanisms that control the exchange through the strait. The dense water transport is topographically controlled and predictions by *Whitehead* [1998] and *Killworth and McDonald* [1993] are consistent with numerical model results. The distribution of temperature and thickness of the modeled plume is in good agreement with the high-resolution hydrographic data.

1. Introduction

The oceanic thermohaline circulation transports large amounts of heat and salt between equatorial and polar regions. Dense water masses are formed mainly at high latitudes before moving equatorward at depth, with lighter water flowing poleward in the upper ocean. There is strong evidence that large changes in the Earth's climate were associated with shifts in the thermohaline circulation. Changes in the deep water formation in the Atlantic sector seem to be a dominant signal associated with climatic changes [e.g., *Ganopolski et al.*, 1998].

In the present climate, Denmark Strait Overflow Water (DSOW) makes an important contribution to the formation of North Atlantic Deep Water (NADW). *Dickson and Brown* [1994] used direct current measurements and hydrographic sections to estimate the transport of water below a defined density level marking the transition to water of overflow origin. The equatorward flow of cold DSOW is strongly affected by the topography of the Denmark Strait. Hydraulic control mechanisms are known to have the potential of limiting the flux of water through straits and over sills [e.g., *Killworth,* 1992a; *Pratt,* 1986].

Large-scale ocean circulation models so far have not succeeded in realistically simulating flow through Denmark Strait. It is likely that this deficiency is caused by the still too coarse resolution of topographic details. For this reason, process models are still useful tools to investigate the role of hydraulic effects in straits. As pointed out by *Whitehead* [1989], most oceanic straits including Denmark Strait may appropriately be viewed as "wide" sills, insofar as they are many Rossby radii across. He used 19 km as Rossby radius in the Denmark Strait approximated as a V-shaped sill with a width of 114 km. *Killworth* [1992b] proceeded to show that, for a single active layer and an infinitely wide or infinitely deep upstream basin, the flow through a "wide sill" occupies only a narrow fraction of the sill.

A number of high-resolution process model studies have already been performed to investigate the formation and dynamics of the dense outflow plume originating from Denmark Strait [e.g., *Jungclaus and Backhaus,* 1994; *Krauss and Käse,* 1998]. These studies concentrated on the flow downstream of the sill. The transport through the strait was usually prescribed as a fixed boundary condition. The present paper presents a process model with a fine numerical grid that includes the region in and upstream of the strait. This model is used to investigate the question what limits exchange through Denmark Strait.

Killworth and McDonald [1993] gave an upper bound for the flux of water across an arbitrarily shaped sill. They related the energy available upstream to the height of the lowest part of the sill topography. A stronger condition for an upper bound was subsequently presented by *Killworth* [1994]. Neither of these arguments is based on hydraulic control. Although it can be shown that in nonrotating systems hydraulically controlled flows are maximal, the role of hydraulic controls under rotation is not assessed easily. The influence of rotation on hydraulically drained flows was discussed for the case of a narrow (with respect to the Rossby radius) sill by *Pratt and Llewellyn Smith* [1997] and *Pratt* [1997]. The latter study also investigated the circulation patterns in the donor and receiver basin. *Killworth* [1995] derived general conditions for hydraulic control in a rotating one-layer reduced gravity system.

2. Idealized Model Configuration

In present hydrostatic ocean circulation models the flow through passages and over sills is not well represented [*Wadley and Bigg,* 1994; *Willebrand et al.,* 2000]. One of the main problems arises from the convective adjustment mechanism used in hydrostatic models to prevent unrealistic statically unstable mean stratifica-

Paper number 2000JC900111.
0148-0227/00/2000JC900111$09.00

tion. During this process, both tracers and momentum are mixed and the entrainment into the plume might be stronger than it would be in reality. The character of the flow is therefore mostly determined by mixing and not by hydraulic or topographic control processes. An improvement can be achieved with models that use bottom following coordinate systems. There are some restrictions on the topographic gradients in order to avoid excess errors in the pressure gradient term, but the general improvement is striking. In this paper we apply such a model (S-coordinate Primitive Equation Model (SPEM) version 5.1). We do not describe the model in detail, since it is well documented [*Song and Haidvogel,* 1994] and applied to several dynamical problems in the literature. The model uses the primitive equations under the hydrostatic approximation on a sigma-coordinate vertical grid. Among the available options to parameterize mixing, we chose simple convective adjustment, horizontal biharmonic mixing and friction with coefficients $A_\rho = A_m = 2 \times 10^9\,\mathrm{m^4\,s^{-1}}$, harmonic vertical mixing with coefficients $K_\rho = K_m = 10^{-3}\,\mathrm{m^2\,s^{-1}}$ for both tracer and momentum, and linear bottom drag (drag coefficients vary among different experiments and are given below).

To access the overflow problem, we first demonstrate that the model is capable of reproducing the basic features of sill flows in a two-dimensional formulation, then proceed to a three-dimensional rotating case with a passage and a sill, and finally look at the Denmark Strait exchange with smoothed but otherwise realistic bottom topography.

2.1. Case $f = 0$

To establish confidence into the results of our numerical model, a first test experiment is set up that approximates a two-dimensional, two-layer flow over a sill without rotation. Here standard hydraulic control theory [e.g., *Armi,* 1986] applies, and we can use analytically derived results to validate the model results. Although the case $f = 0$ is only meant to be an initial test, we try to set up a model configuration that takes into account some aspects of the situation at Denmark Strait: a single sill is considered with inflow of cold water in the upstream reservoir at a rate much higher than that eventually carried over the sill.

The neglect of rotation reduces the problem to two space dimensions. (Strictly speaking, the numerical grid of the model does not allow for two-dimensional problems. This was accounted for by using a very narrow slab only three grid points wide with free-slip boundary conditions.) The model domain is a two-dimensional (2-D) basin with a maximum depth of

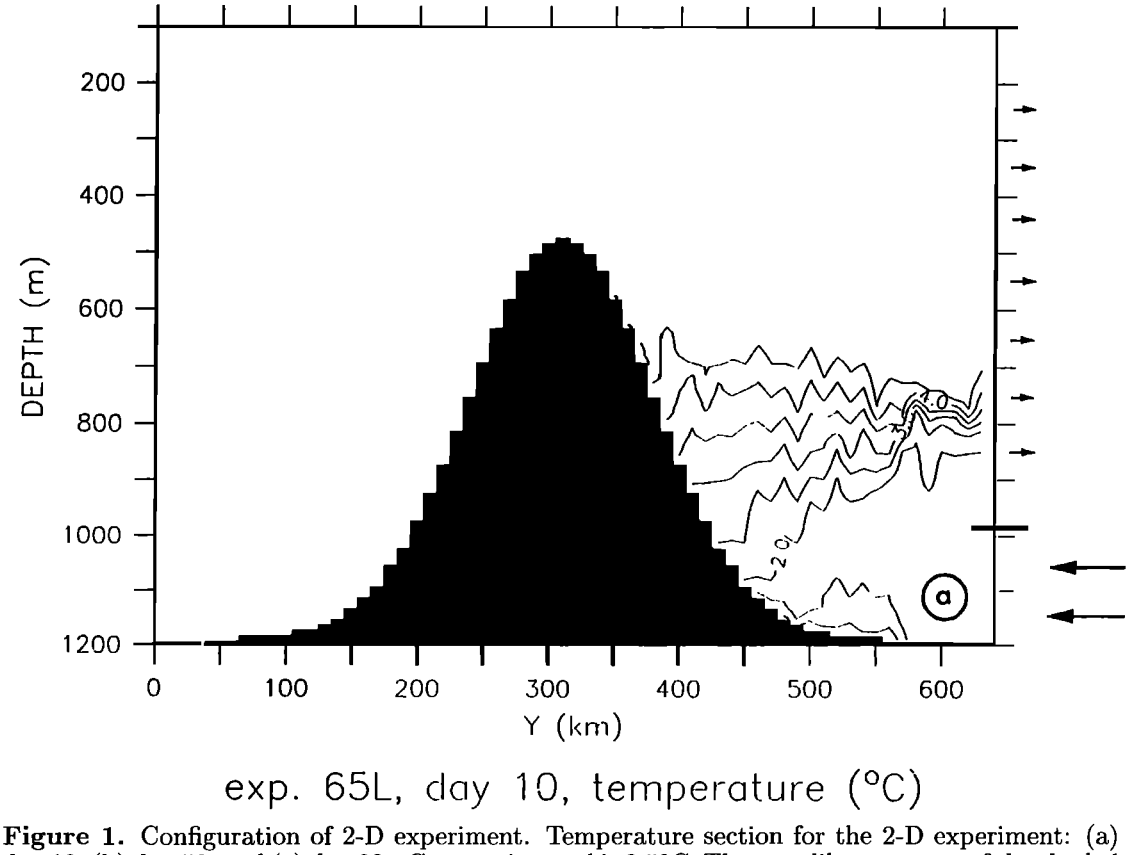

Figure 1. Configuration of 2-D experiment. Temperature section for the 2-D experiment: (a) day 10, (b) day 50, and (c) day 90. Contour interval is 0.5°C. The step-like structure of the shaded topography is an artifact of the plotting program. Due to its sigma-coordinate formulation, the topography in the SPEM model exactly follows the analytical gaussian shape. The arrows on the right-hand side of Figure 1a indicate regions of prescribed inflow and outflow.

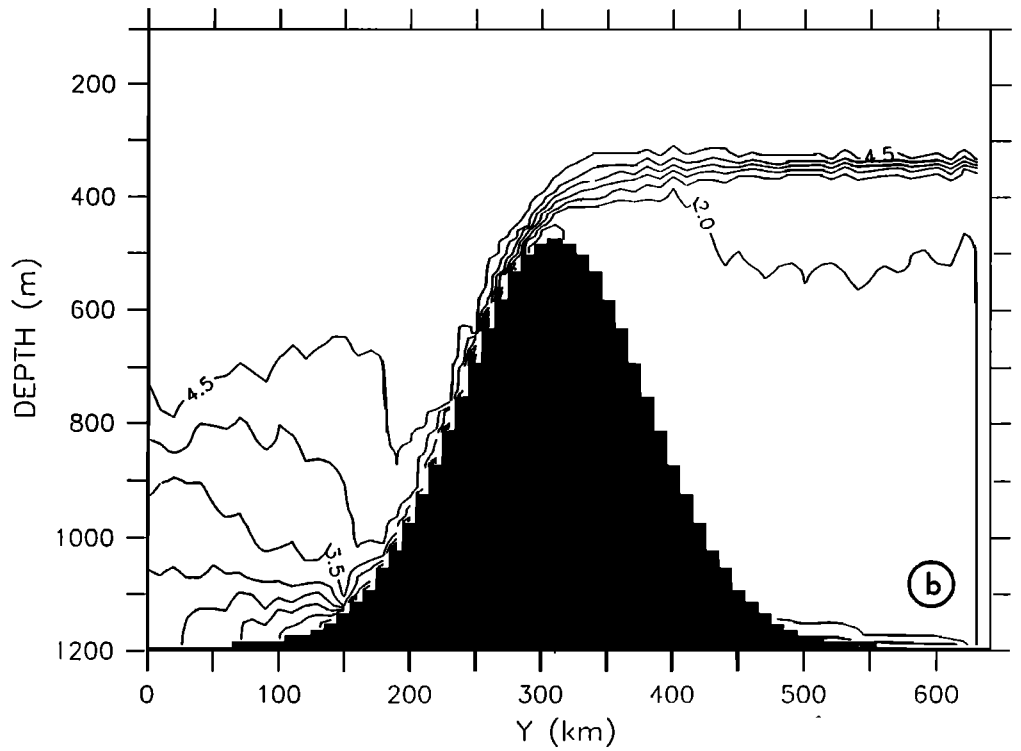

exp. 65L, day 50, temperature (°C)

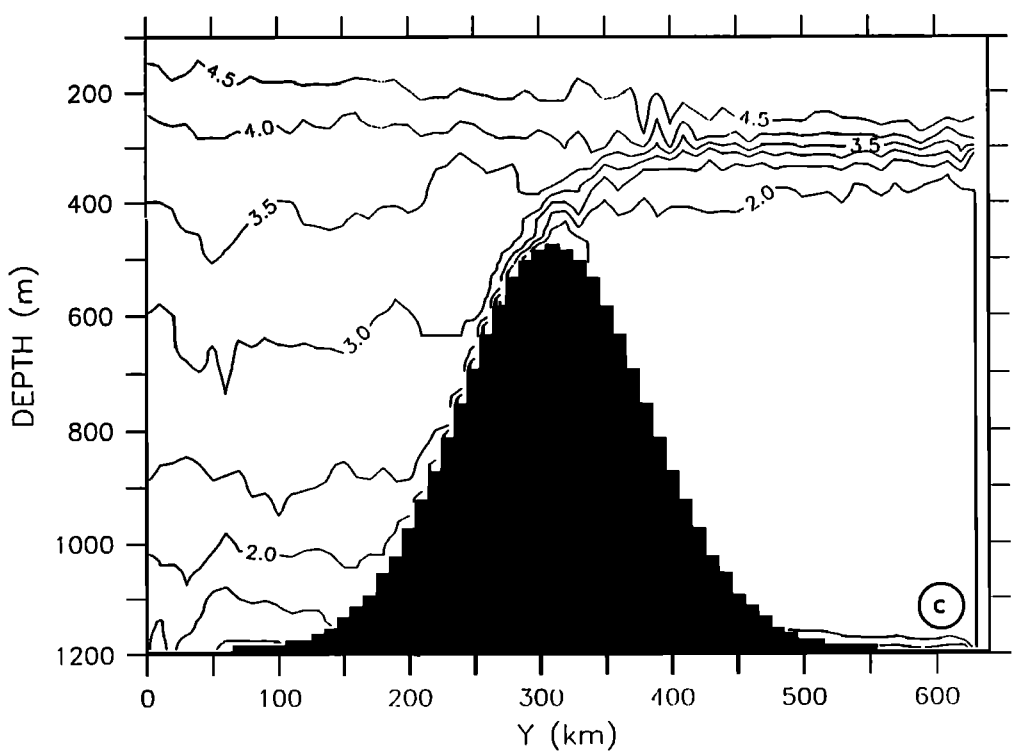

exp. 65L, day 90, temperature (°C)

Figure 1. (continued)

$H_{max} = 1200\,m$ that extends over 650 km in the horizontal and which contains a Gaussian sill centered at $x = 325\,km$ with half width of 163 km and a sill depth of $H_{sill} = 480\,m$ (Figure 1). The grid spacing is 10 km in the horizontal and 65 almost evenly spaced sigma levels in the vertical (with levels toward top and bottom becoming thinner by not more than 10% of the average local layer thickness).

The model is initialized with a homogenous temperature of 5°C. At $t = 0$, water begins to flow in uniformly over the depth range 990 to 1200 m at the boundary at $x = 650\,km$ with prescribed velocity ($55.65\,cm\,s^{-1}$) and temperature (2°C). The compensating outflow is distributed uniformly over the top 990 m at the same boundary with uniform velocity ($11.8\,cm\,s^{-1}$) but free temperature. Salinity effects are neglected, and a linear equation of state is used with density anomalies resulting from temperature alone. The temperature coefficient of $-0.14 \times 10^{-3}\,°C^{-1}$ results in a density contrast of $0.42\,kg\,m^{-3}$ and a reduced gravity of $g' = 0.0041\,m\,s^{-2}$.

What will happen if we let cold water flowing in at the bottom? First, the right-hand basin will fill up with cold water underlying the warmer and lighter 5°C water. Because of the outflow all along the right-hand boundary above the lower 210 m, the net inflow of cold water will decrease with increasing height of the interface between cold and warm water. When the sill depth is reached, cold water will start flowing into the receiving basin. Eventually, the volume flux of cold water across the sill will equal the net inflow of cold water and the interface ceases to rise. Were the receiving basin infinitely large, a steady state would persist. Due to the limited model region, we have to expect effects arising from the accumulation of cold water in the receiver basin.

Figure 1 shows the time evolution of the temperature field, with the corresponding velocities shown in Figure 2. The actual topography of the sigma-coordinate model consists of piecewise constant slopes, in contrast to the step-like pattern shown in the plots that results only from interpolation of the model data from σ to z levels for the purpose of visualization.

At day 10 the cold water has not yet reached the sill depth. Note, however, that due to numerical overshooting related to the use of a central-difference advection scheme, water colder than 2°C is found close to the inflow at the bottom. At day 50 the level of cold water in the donor basin is about 100 m above sill height. A narrow overflow over the sill has developed that allows cold water to pass without much mixing into the left basin. Overflow velocities exceed $80\,cm\,s^{-1}$, and the thickness of the overflow water along the sill is less than 100 m. Mixing becomes more intense close to the downstream boundary and results in a much more diffuse thermocline than in the upstream basin. The enhanced vertical

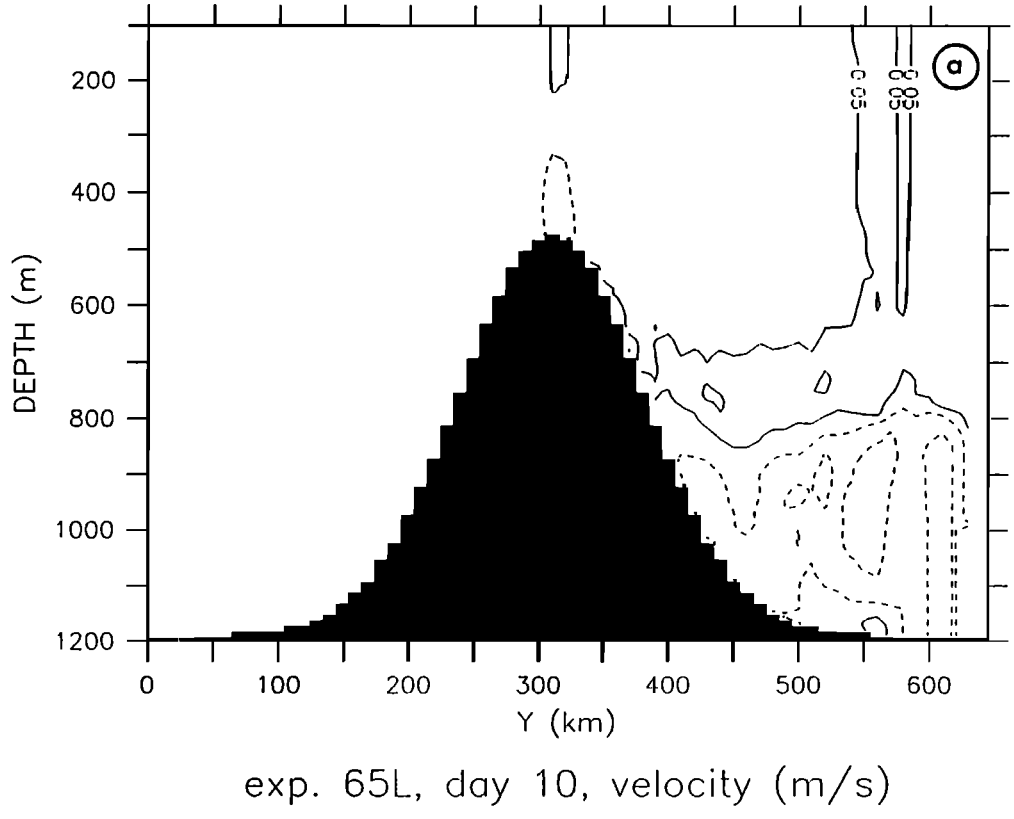

Figure 2. Velocity section for the 2-D experiment: (a) day 10, (b) day 50, and (c) day 90. Contour interval is $0.1\,m\,s^{-1}$.

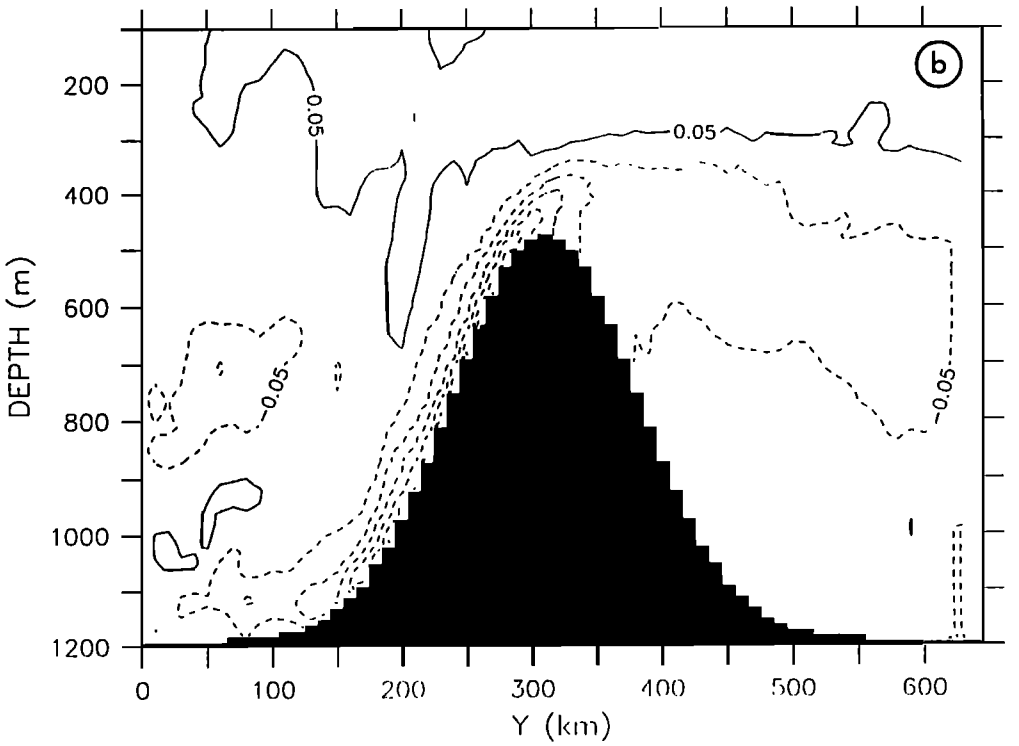

exp. 65L, day 50, velocity (m/s)

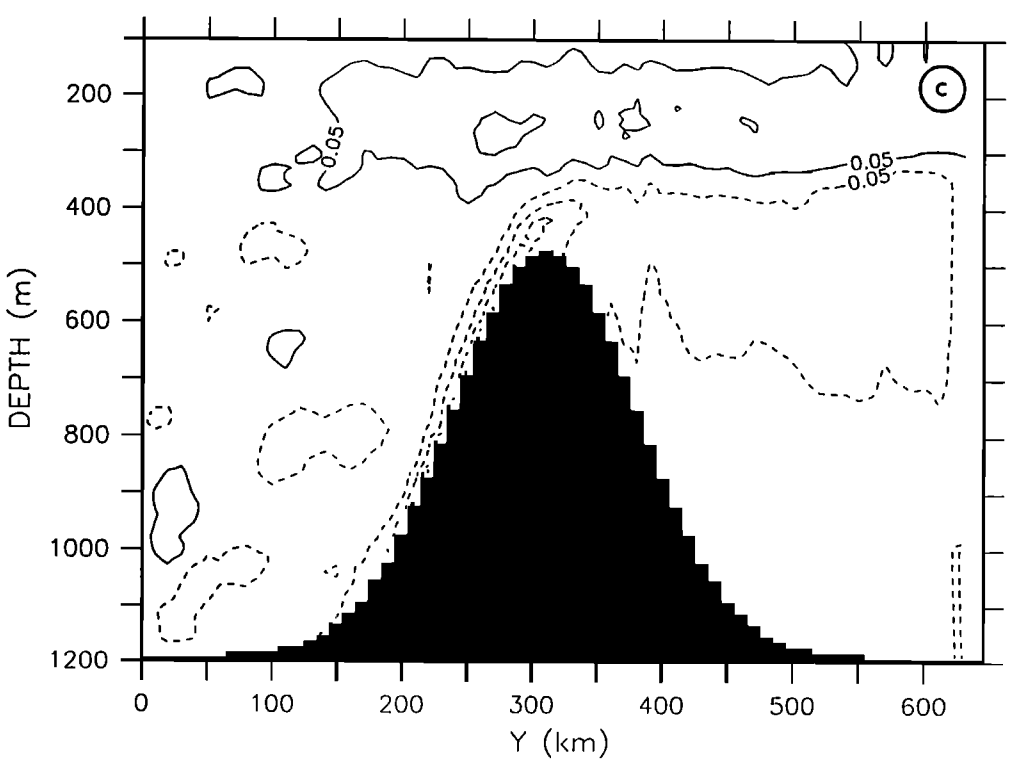

exp. 65L, day 90, velocity (m/s)

Figure 2. (continued)

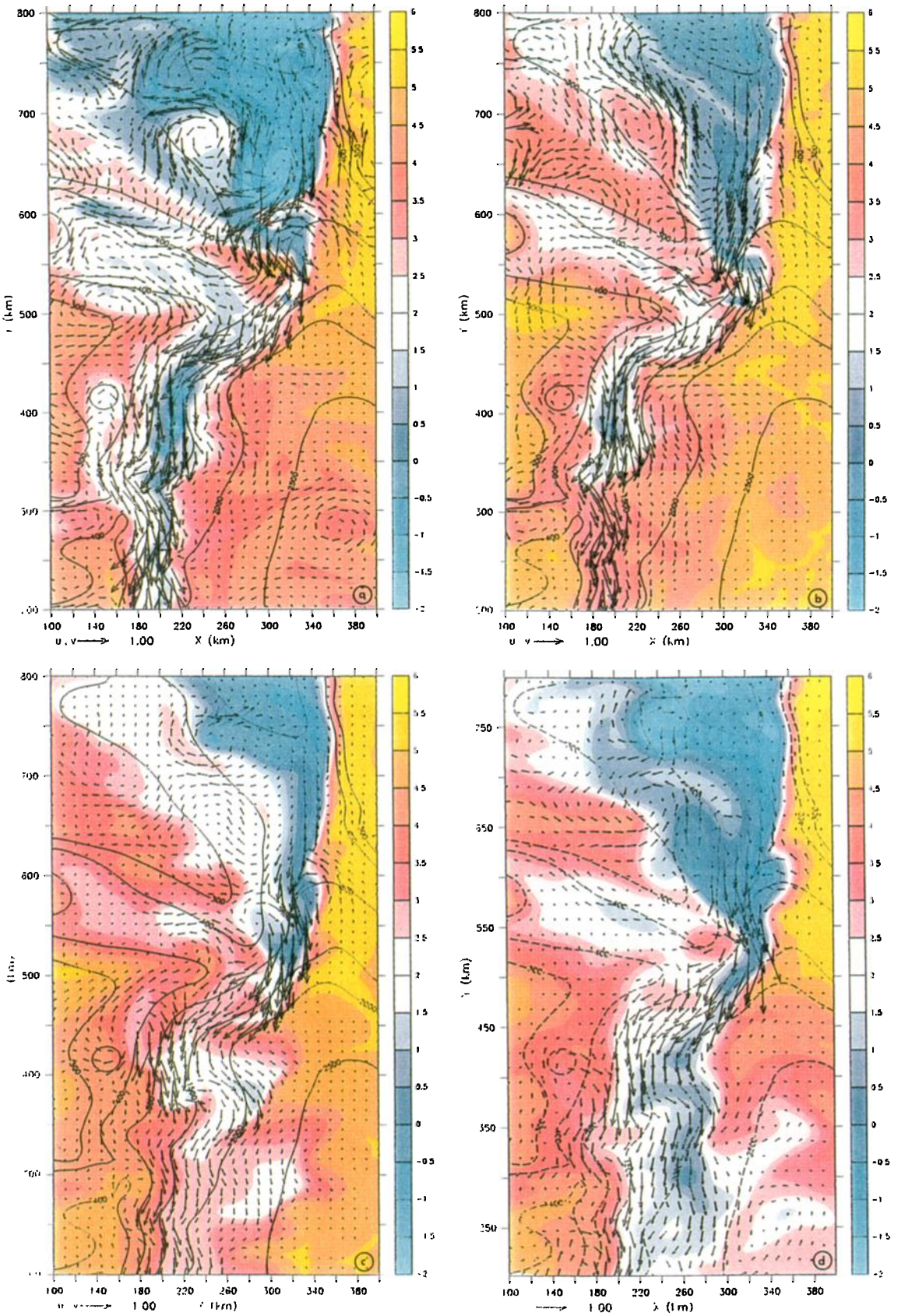

Plate 1. (a) Instantaneous snapshot of bottom temperature and velocity vectors for run RCL with $r_d = 4.15 \times 10^{-5}$. (b) Instantaneous snapshot of bottom temperature and velocity vectors for run RWL with $r_d = 4.15 \times 10^{-5}$ and 1°C warmer source temperature than in Plate 1a. (c) Instantaneous snapshot of bottom temperature and velocity vectors for run RWH with $r_d = 4.15 \times 10^{-4}$ and 1°C warmer source temperature than in Plate 1a. (d) Instantaneous snapshot of bottom temperature and velocity vectors for run RCH with $r_d = 4.15 \times 10^{-4}$.

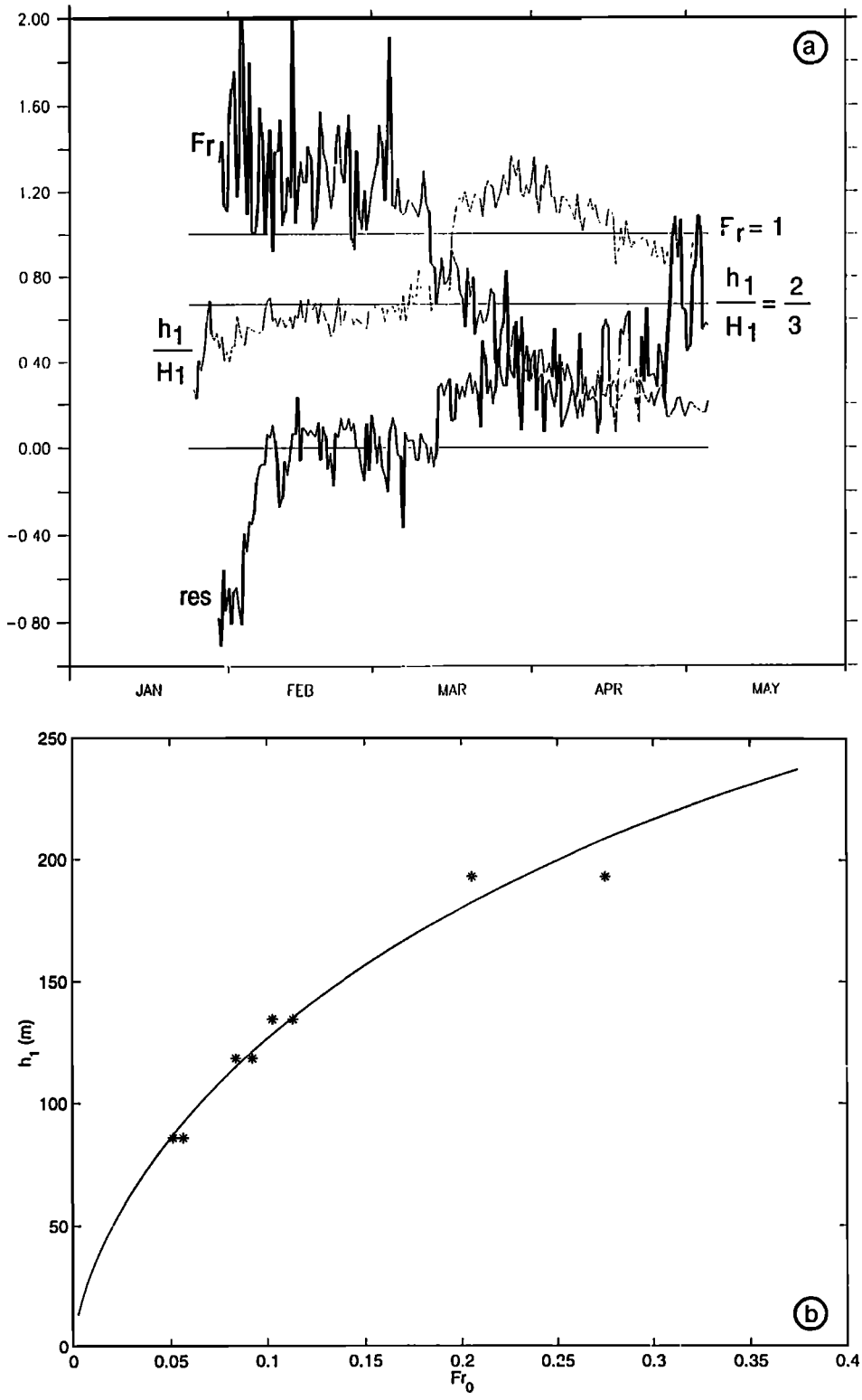

Figure 3. (a) Froude number Fr at $x = 290$ km just downstream of the sill; interface height at the sill h_1 normalized with the reservoir height above sill H_1 (equation (2)). Also shown is the residual (res) of (6) for values of ξ calculated by the circulation model. The three horizontal lines refer to the critical Froude number $Fr = 1$, $h_1/H_1 = 2/3$, and the zero line corresponding to the right-hand side of (6). (b) Dependence of model interface reservoir height as function of the scaling Froude number Fr_0 for four different experiments (asterisks). For each experiment, results are given according to the upper and lower bounds of the interface definition. The solid line refers to the exact solution of (6).

mixing is a combined effect of the presence of a vertical wall and the development of a hydraulic jump. At day 90 the 4°C isotherm is situated about 180 m above the sill depth in both basins. Still, a narrow overflow band of cold water is present down the slope of the sill, with maximum velocities larger than $50\,\mathrm{cm\,s^{-1}}$. Note that at days 50 and 90 a deep recirculation cell has developed in the upstream reservoir (Figures 2b and 2c), indicating that the inflow is larger than the flow over the sill.

Assuming that the flow across the sill is subject to hydraulic control implies a Froude number being order of unity. Here the Froude number is defined to be that of a two-layer system, $Fr^2 = (u_1)^2/(g'h_1) + (u_2)^2/(g'h_2)$, where u_i is the velocity of layer i, g' is the reduced gravity, and h_i is the respective layer thickness. The sharp thermocline seen in Figure 1 above the sill justifies this two-layer approximation. The temporal evolution of this number is shown for a grid point (at $y = 290\,\mathrm{km}$) just downstream of the sill in Figure 3a. Fr is not defined prior to day 30 when the cold water reaches the sill depth and the overflow starts. While Fr is always less than 1 right at the sill (at $y = 310\,\mathrm{km}$, not shown), it exceeds unity some 20 km downstream at $y = 290\,\mathrm{km}$ between days 30 and 75, indicating that the flow is hydraulically controlled. The displacement of the control point in the direction downstream of the sill is due to bottom friction [*Pratt*, 1986].

The relevant dynamic relation is Bernoulli's law, for a two-layer system given as

$$B = \frac{1}{2}\left(u_1^2 - u_2^2\right) + g'd_1 + g'h = \mathrm{const}\,, \qquad (1)$$

with u_1 and u_2 referring to the velocities in the two layers, h is the height of the bottom topography, and d_1 is the thickness of the lower layer. Strictly speaking, Bernoulli's law only applies to stationary nonviscous flow. Since we have reduced friction in the model to values as small as possible, we may assume that friction terms are small in the relevant dynamical balances. The validity of this approach will be proven below when we discuss the residuals of the frictionless equation. In the following we use capital letters for properties in the donor basin and small letters for properties at the sill.

For the situation presented by our model configuration we have $u_1^2 \gg u_2^2$, that is, we can neglect the upper-layer return flow. Since B is constant along a streamline, (1) relates sill and upstream basin:

$$\frac{1}{2}u_1^2 + g'h_1 = g'H_1\,, \qquad (2)$$

where we have neglected the kinetic energy part in the upstream basin, and where H_1 refers to the "depth over sill" of the cold layer in the upstream basin, that is, that part of the layer that lies above the sill depth.

If the flow across the sill is critical, then the Froude number, $Fr = u_1/\sqrt{g'h_1}$, becomes unity at the sill. From (2) it then follows that

$$H_1 = \frac{3}{2}h_1\,. \qquad (3)$$

Since in our model configuration the upper layer of warm water must exactly compensate the overflow of cold water across the sill, and since for continuity this transport also equals the outflow of warm water at the right-hand boundary, we have

$$u_2 d_2 = -u_1 h_1 = U_2 H_2\,. \qquad (4)$$

Because U_2 is the known outflow velocity (here $11.8\,\mathrm{cm\,s^{-1}}$) and $H_1 + H_2 + H_{\mathrm{sill}} = H_{\mathrm{max}} = 1200\,\mathrm{m}$, we can combine (3) and (4) to obtain

$$\sqrt{g'}\left(\frac{2}{3}H_1\right)^{3/2} = U_2\left(H_{\mathrm{max}} - H_{\mathrm{sill}} - H_1\right)\,. \qquad (5)$$

With g', H_{max}, H_{sill}, and U_2 given by the geometry,

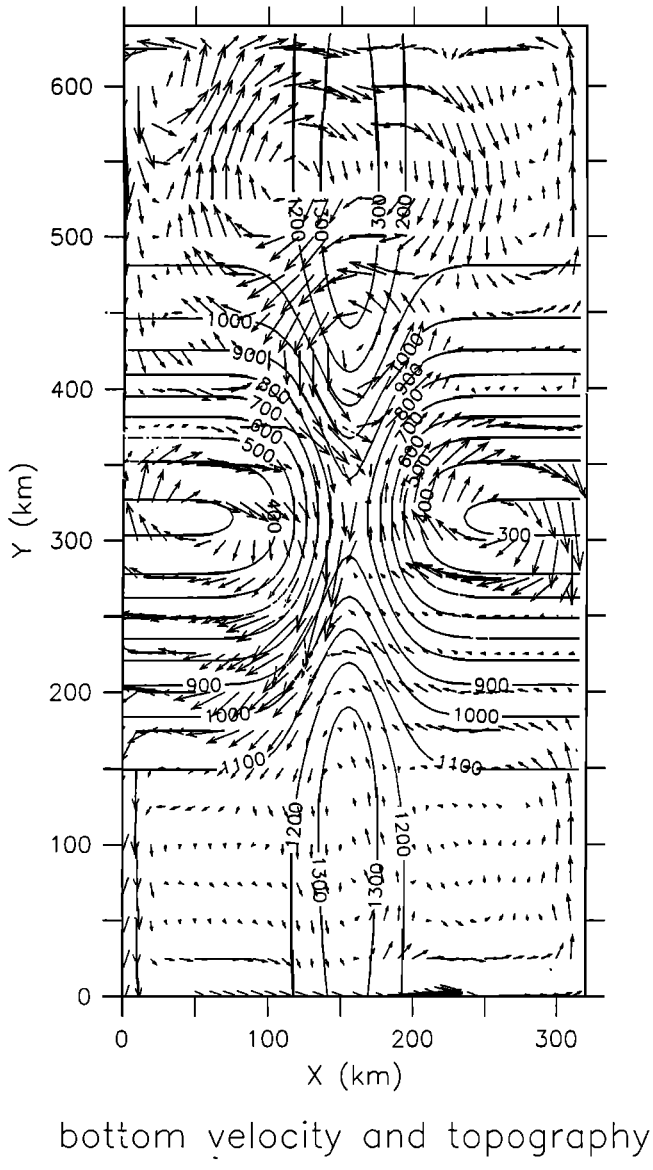

Figure 4. Bottom topography for the idealized $f \neq 0$ experiment. The arrows denote the bottom velocity averaged over days 50 to 70.

we can solve the above cubic equation in $\sqrt{H_1}$. If we scale this equation by $U_2\,(H_{\max} - H_{\sill})$, we obtain an algebraic equation for $\xi = \sqrt{H_1}/\,(H_{\max} - H_{\sill})$:

$$\left(\frac{2}{3}\right)^{3/2} Fr_0^{-1}\xi^3 + \xi^2 - 1 = 0\,, \qquad (6)$$

where $Fr_0 = U_2/\sqrt{g'\,(H_{\max} - H_{\sill})}$ is a scaling Froude number based on the full water depth at the sill.

The solution to this equation as a function of Fr_0 is displayed in Figure 3b. To verify this functional dependence, we have included H_1 and Fr_0 generated by four independent runs with varying inflow parameters of the 2-D model. It turns out that in the low Fr_0 range ($Fr_0 < 0.2$) the sensitivity of H_1 to upstream changes is approximately proportional to $U_2^{2/3}$ and to $g'^{-1/3}$. For higher values of Fr_0 the dependence of H_1 on U_2 and g' is even weaker.

2.2. Case $f \neq 0$

A second idealized model configuration adds another space dimension. It combines a sill and a contraction and also accounts for rotation. Figure 4 displays the configuration of the model which has a resolution of 10 km in the horizontal and 12 sigma levels (with almost even spacing) in the vertical. Close to the western wall, an inflow of 6.6 Sv of water with a temperature of 0.5°C is introduced at the northern boundary (with a velocity of 51 cm s^{-1} in the lower 325 m). A compensating outflow is applied in the water column above the inflow. At the southern boundary we impose an inflow of identical magnitude (6.6 Sv): warm water (5°C) flowing in over the upper 875 m close to the eastern wall, with compensating outflow at the bottom. Thus at both northern and southern boundaries an overturning transport of 6.6 Sv is prescribed.

Corresponding to the $f = 0$ experiment of the previous section, the basin is initially filled with homogeneous water of 5°C. Again, salt is not included, and the same linear density function is used. After time $t = 0$ the northern basin starts to fill up with cold water that reaches the sill at about day 10. Zonal sections of temperature (Figure 5) and meridional velocity (Figure 6) right at the sill, averaged over the period day 50 to day 70, show southward flow of cold water through the channel as well as of warm water across the shelf at the eastern wall. Since we are interested only in the flow through the channel, we use the 4°C isotherm as criterion to discriminate the cold southward flow through the channel from warmer water flowing northward across the shelf.

The corresponding flow in the bottom layer is shown for the entire basin in Figure 4. The confinement of the overflow to the western flank of the sill is a result of the presence of rotation. The horizontal width of the overflow is governed by the Rossby radius, for a reduced gravity flow given by $R = \sqrt{g'h_1}/f$, where h_1 is the thickness of the overflow layer and f the Coriolis

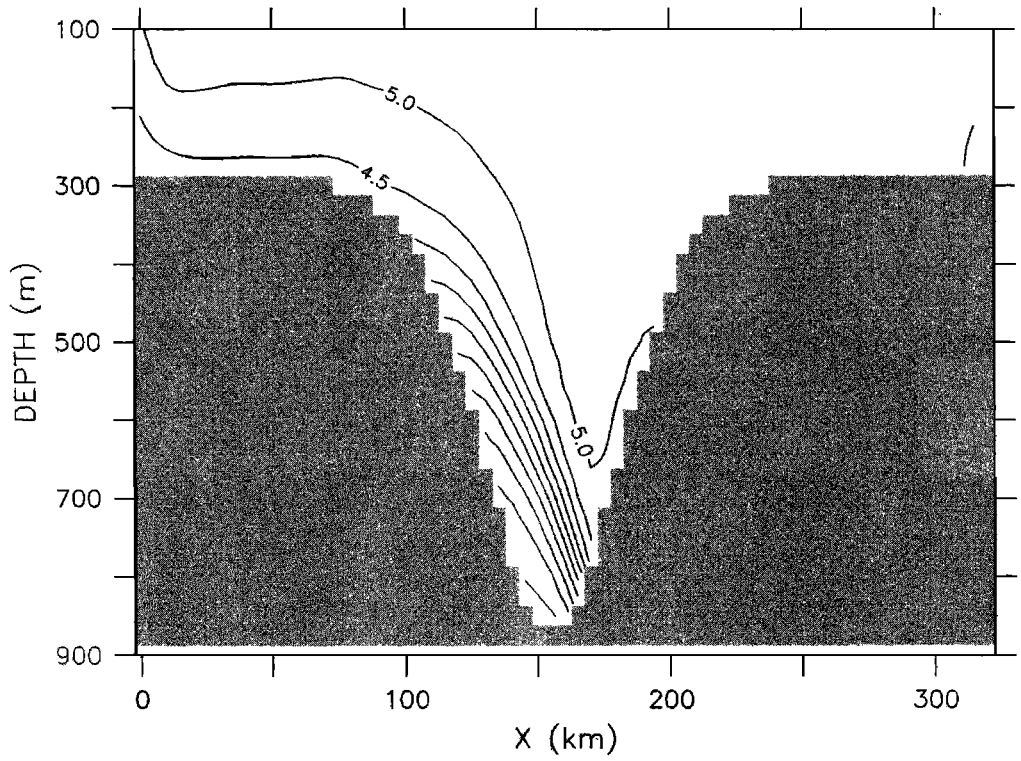

Figure 5. Zonal temperature section at the top of the sill, averaged over days 50 to 70. Units are °C.

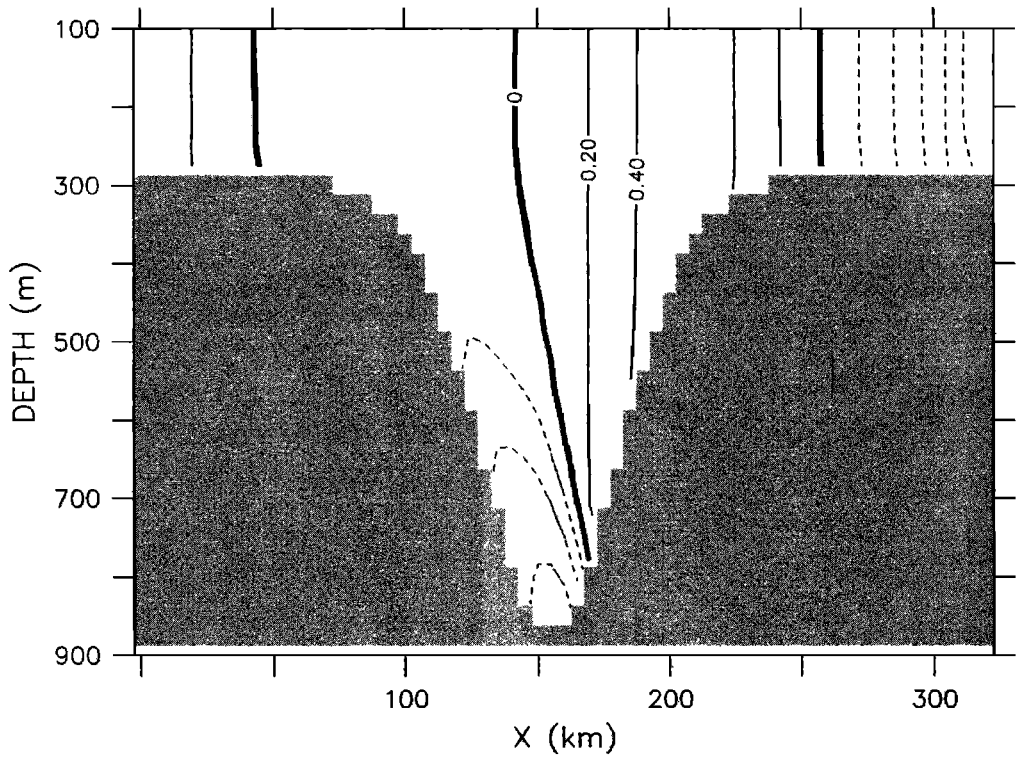

Figure 6. Zonal section of meridional velocity at the top of the sill, averaged over days 50 to 70. Units are $\mathrm{m\,s^{-1}}$.

parameter. As is applicable for Denmark Strait, the sill width in our simple box model is larger than the Rossby radius, allowing for an exchange flow separated by an almost vertical front in the strait.

Another effect of rotation is the vigorous circulation in the northern basin. In contrast to the $f = 0$ case dealt with in the previous section it is now no longer obvious how a water column at the northern boundary is connected with the flow at the sill [*Pratt and Llewellyen Smith*, 1997; *Pratt*, 1997]. In our analysis based on the Bernoulli function we therefore include the kinetic energy term throughout and in addition to the height over sill, H_1, considered in the $f = 0$ case, we define an effective height over sill, H_{eff}, by the conserved quantity

$$g' H_{\mathrm{eff}} = \frac{1}{2} u_1^2 + g' H_1 \ . \tag{7}$$

For the 4°C isotherm, taken to represent the thermocline that separates cold and warm waters, the effective height over sill is displayed in Figure 7. It turned out that despite the circulation in the northern basin there is still a close similarity between H_1 and H_{eff} away from the sill.

Killworth and McDonald [1993] gave an upper limit of the volume transport of a steady flow through sills:

$$\Psi_{\max} = \frac{1}{2} \frac{g' H_{\mathrm{eff}}^2}{f} \ . \tag{8}$$

Here H_{eff} should be computed for the flow upstream of the overflow. In the model experiment the area $360\,\mathrm{km} < y < 420\,\mathrm{km}$ was chosen to compute a mean H_{eff}. A time series of the predicted maximum transport $\Psi_{\max}$ is shown in Figure 8 together with the diagnosed overflow of water colder than 4°C across the sill. Although the steady flow condition for relation (8) is not strictly met, predicted and simulated transport show a very similar evolution during the first 6 months of the experiment. Major discrepancies develop only after the cold water in the northern basin has risen to a level where it begins to spill over the shelves into the southern basin (end of May).

In the nonrotating case (section 2.1), we found a very weak dependence of the interface height at the sill (and hence of the transport) on the temperature of the overflow water (equation (5)). To test whether this result still applies to the rotating case, we have repeated the $f \neq 0$ run with the temperature of the inflowing water raised by 0.5°C. The corresponding predicted and simulated overflow transports are included in Figure 8 and confirm the very weak dependence of the transport on the temperature of the overflow water.

3. Simulation With Realistic Topography

Due to its wide sill character (width scaled with Rossby radius much larger than unity), the Denmark Strait develops an almost vertical front between Icelandic and Greenland waters. The interbasin exchange

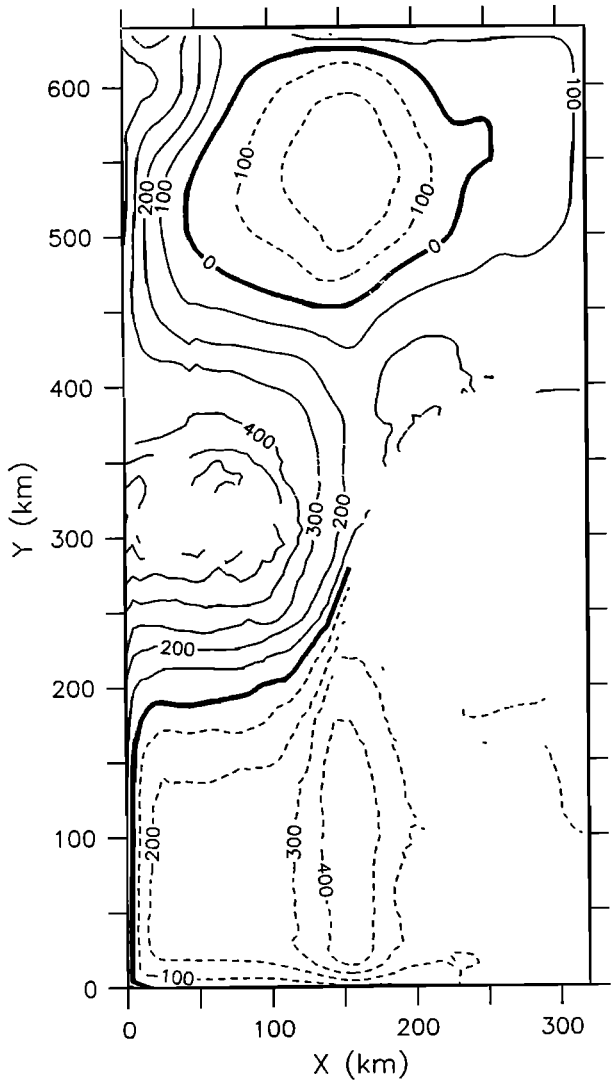

Figure 7. Effective depth H_{eff} of the 4°C isotherm averaged over days 50 to 70. Units are meters.

thus does not really happen in a vertical cell, but rather in a horizontal one. This requires a horizontal resolution sufficient to resolve the vorticity dynamics of two separated narrow currents. Figure 9 shows the geometry and bathymetry of the model region. Note that the presentation is on a rectangular grid with curved geographical coordinates. The model domain consists of 130 × 210 × 31 grid points. The average grid spacing is 4.3 km in both horizontal directions. With 31 σ levels, the vertical resolution on the sill is about 20 m. At 1500 m depth the overflow plume can still be resolved by 50 m thick layers, while at the greatest depth the spacing increases to 100 m.

For simplicity the coastlines are neglected and the shelf areas are limited to a minimum depth of 150 m. The domain is closed except at the northern wall (j = 210), where we allow a 10 × 15 grid points wide inflow at cells $i = 55 - 65, k = 1 - 15$ of -1°C cold water into the initially homogeneous fluid of 5°C temperature. The inflow speed of $0.3566\,\mathrm{m\,s^{-1}}$ amounts to 8.3 Sv transport of dense water into the basin north of the sill. The same volume of water is forced to leave the area by requiring zero volume transport at each column of boundary-transport points. A linear equation of state is used as in the previous experiments with density anomaly resulting from temperature alone. The temperature coefficient of $-0.14 \times 10^{-3}\,^{\circ}\mathrm{C}^{-1}$ results in a density contrast of 0.84 σ units and a reduced gravity of $0.0082\,\mathrm{m\,s^{-2}}$. This corresponds to a Rossby radius of 11 km for a 300 m thick overflow plume. The density difference would yield a maximal throughflow of 2.5 Sv for a reservoir height of 300 m above the sill depth according to *Whitehead* [1998]. The inflow is supermaximal, and if hydraulic/topographic control should occur, a considerable amount of dense fluid must recirculate in the northern basin.

As in the previous model runs we use the biharmonic friction option of SPEM for temperature and momentum. Taking into account that most of the flow will be bottom parallel, we do not rotate the mixing tensor. Diffusion will therefore be along the generalized sigma surfaces. Several tests involving *Pacanowski and Philander* [1981] type Richardson number dependent mixing as well as mixing according to *Mellor and Yamada* [1982] did not produce drastic changes in the results regarding transport behavior. Use of a simple convective adjustment scheme makes it possible to directly compare the results with those of the DYNAMO experiments [*Willebrand et al.*, 2000].

In the following we will discuss results from four different configurations: A reference run with inflow temperature of −1°C and high bottom drag $r_d = 4.15 \times 10^{-4}\,\mathrm{m\,s^{-1}}$ (referred to as RCH, an abbreviation for run-cold-high), a configuration of RCH but a 10 times smaller bottom drag (referred to as RCL, run-cold-low). Runs 3 and 4 use a 1°C warmer inflow with $r_d = 4.15 \times 10^{-4}\,\mathrm{m\,s^{-1}}$ (referred to as RWH, run-warm-high) and $4.15 \times 10^{-5}\,\mathrm{m\,s^{-1}}$ (referred to as RWL, run-warm-low).

The bottom temperature of RCL and RWL after 3 months inflow is shown as an instantaneous snapshot upstream and downstream of the Denmark Strait sill (Plates 1a and 1b). The dense water which has accumulated upstream on the Icelandic side is crossing the sill on the East Greenland slope with velocities larger than $1\,\mathrm{m\,s^{-1}}$. This flow pattern is reminiscent of *Whitehead*'s [1989] rotating hydraulics results. Further downstream a substantial fraction spills directly into a channel system (the Storfjord Deep) off the Dohrn Bank (see Figure 9 for location). The flow out of this channel is mixed with shelf waters and shoots back into the slope current, disrupting the continuous outflow.

The area south of Dohrn Bank plays a substantial role in eddy formation. Here the main descent of the plume with large downslope overshooting and supercritical flow takes place. An analysis of the Froude number indeed shows values larger than unity in a 40-50 km

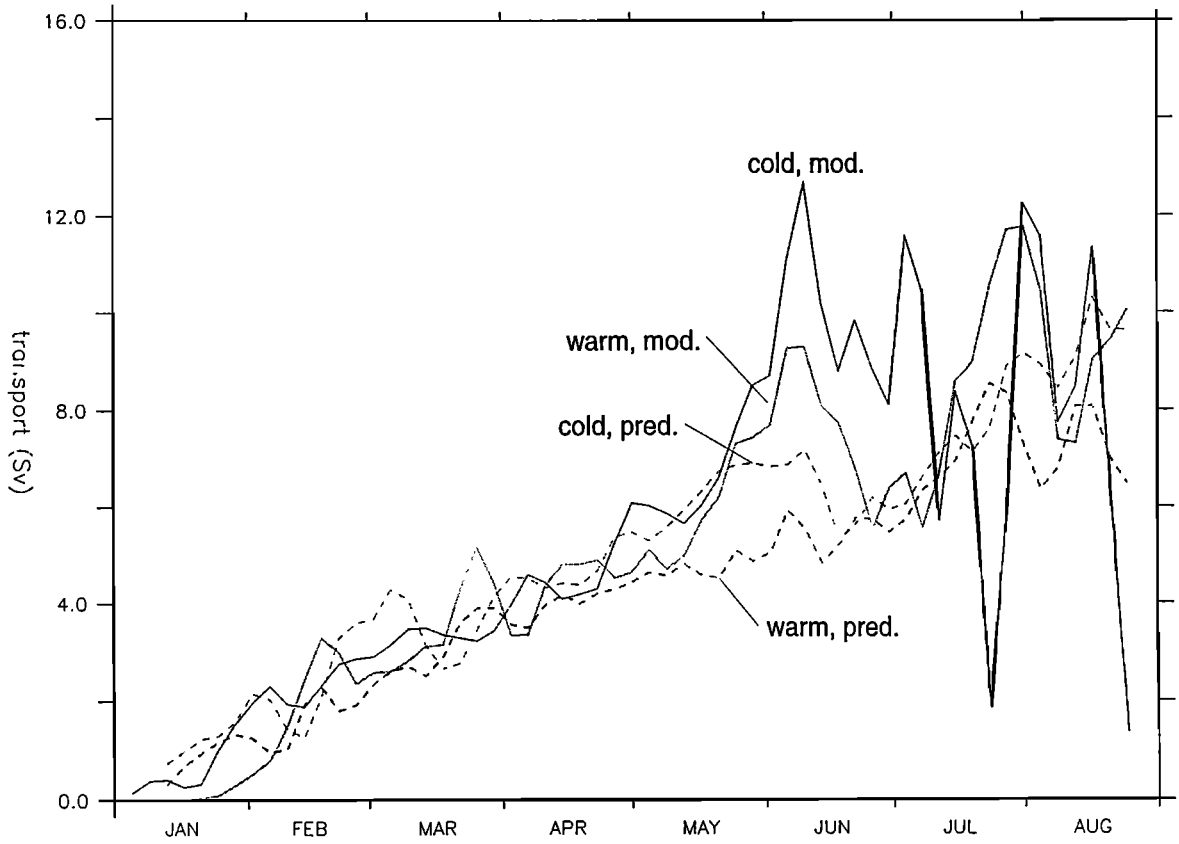

Figure 8. Temporal evolution of the volume transport of water colder than 4°C across the sill (solid line) and volume transport predicted by (8) (dashed line). Thick lines refer to the standard experiment with the temperature of the inflowing water set to $T_{\text{inflow}} = 0.5°\text{C}$, and the thin lines are the results from a sensitivity experiment with $T_{\text{inflow}} = 1°\text{C}$.

wide and 120 km long area of the downslope flow centered at the location $x = 315\,\text{km}$ and $y = 550\,\text{km}$ (Figure 10). The transition from supercritical to subcritical flow seems to be a preferred site of mixing and eddy formation. Note that the current vectors in Figure 10 are 4 months mean values calculated for the period April to July. Individual maps of the Froude number show much larger values and more localization. It is obvious that parameterization of the bottom boundary layer in this region will be crucial for the mixing and forming of the new deep water mass.

It is interesting in this context to compare the core location at the same bottom drag for the cool and the warm runs. For the low bottom drag there is no apparent difference in the location of the overflow core. After the flow has adjusted to geostrophy, the main jet is guided by the region of highest bottom slope s, because there the topographic speed $g's/f$ is maximal [*Nof*, 1983]. This situation is changed when high bottom drag is applied (Plate 1c). After 20 days further integration of RWL, but with high bottom drag, the eddies have spread the overflow water down to depths greater than 2000 m. After 6 months of integration of run RCH much of the Irminger Sea deep basin is showing temperatures between 2°C and 3°C and steady translation of eddy chains (Plate 1d). Since the emphasis of this paper is on the role of topographic control, we do not discuss the downstream behavior in more detail but address now the transport limitation.

As shown above, the through flow is controlled by the upstream height above the sill level with little influence of the kinetic energy of the flow. The sill transports as function of time for the four cases are shown in Figure 11a as well as the scaled transports (Figure 11b). After a 3 months spin up with only small eddy variations, the flow through the sill is controlled by pulsating events around the predicted maximal Whitehead-Killworth transport. It is interesting to note that there is not much variation for the different cases. This was expected, because the sensitivity to changed inflow density is only weakly depending on the source density. The maximal through flow criterion nevertheless deserves some closer inspection. Since we have used an average effective height in the sill entrance, there is a tendency for the maximal hydraulic flow to be underestimated, leading to some values larger than unity in the normalized transports. We have tried several different definitions of the effective height and found the best agreement by visual inspection of the streamlines and use of the maximal value for the Bernoulli func-

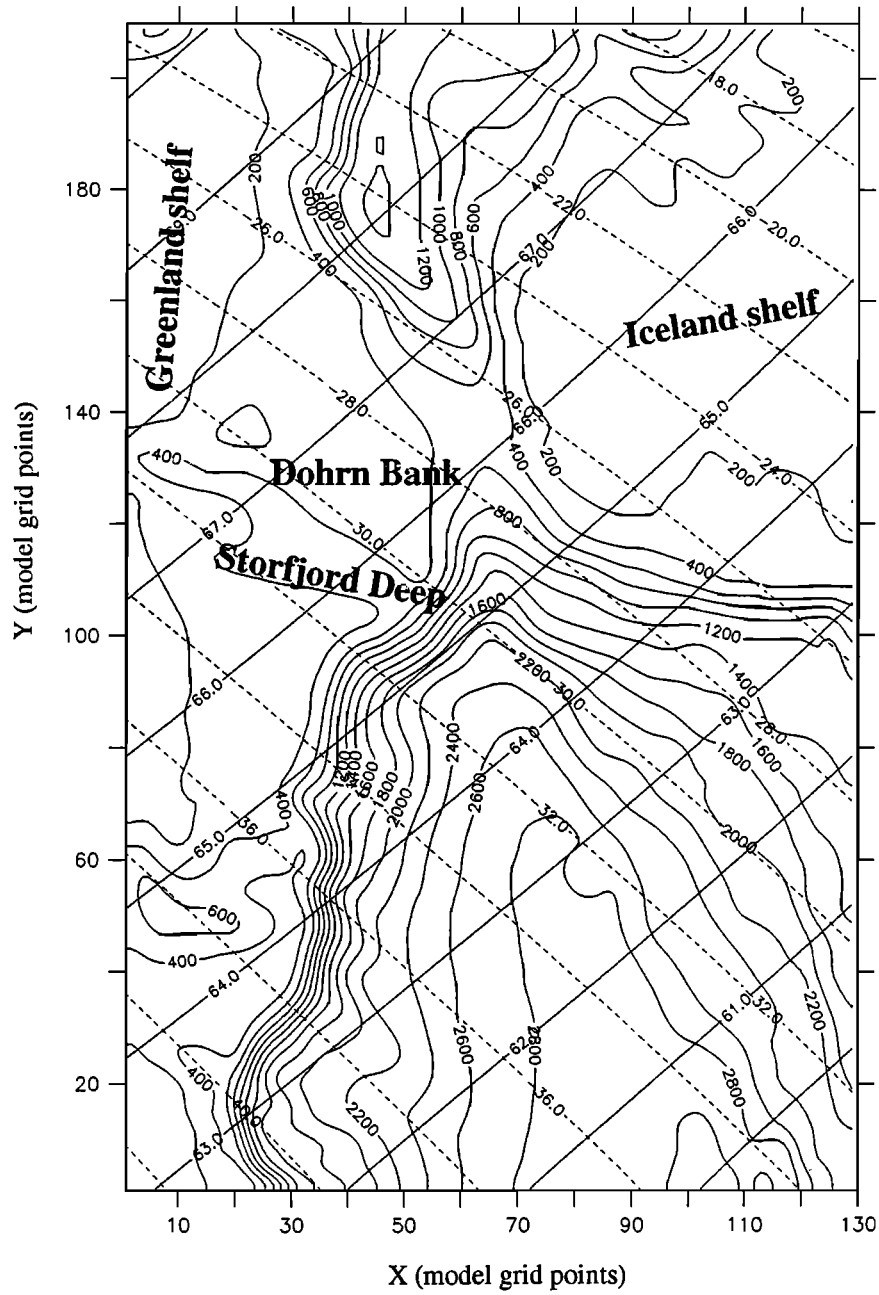

Figure 9. Bottom topography (in meters) and geographical location of the model domain.

tion. In practice, this requires the exact flow structure upstream, which is hardly feasible for observations. Obviously, the suggestion of *Whitehead* [1998] to use just two stations for the transport leads to good results for the flow prediction (Figure 11c).

An anonymous reviewer suggested to compare the above results with an experiment with simple dam-break initial conditions. North of the sill the basin is initially filled with cold (-1°C) water up to $z = 100$ m above which warm (5°C) water resides that also fills the entire basin south of the sill. The results of two dam-break experiments are displayed in Figure 11d that shows the evolution of the normalized transport for low and high bottom-friction parameters corresponding to runs RCL and RCH above. Obviously, the resulting normalized transport is generally less than 1, which may be related to the fact that in the dam-break configuration there is not sufficient time to establish a relatively steady condition in both flow and interface height.

4. Comparison With Observations

The general distribution of the model bottom plume is remarkably consistent with ship observations, which were obtained during Poseidon cruises in 1996 and 1997 (Plate 2). The overflow plume descends from 600 m

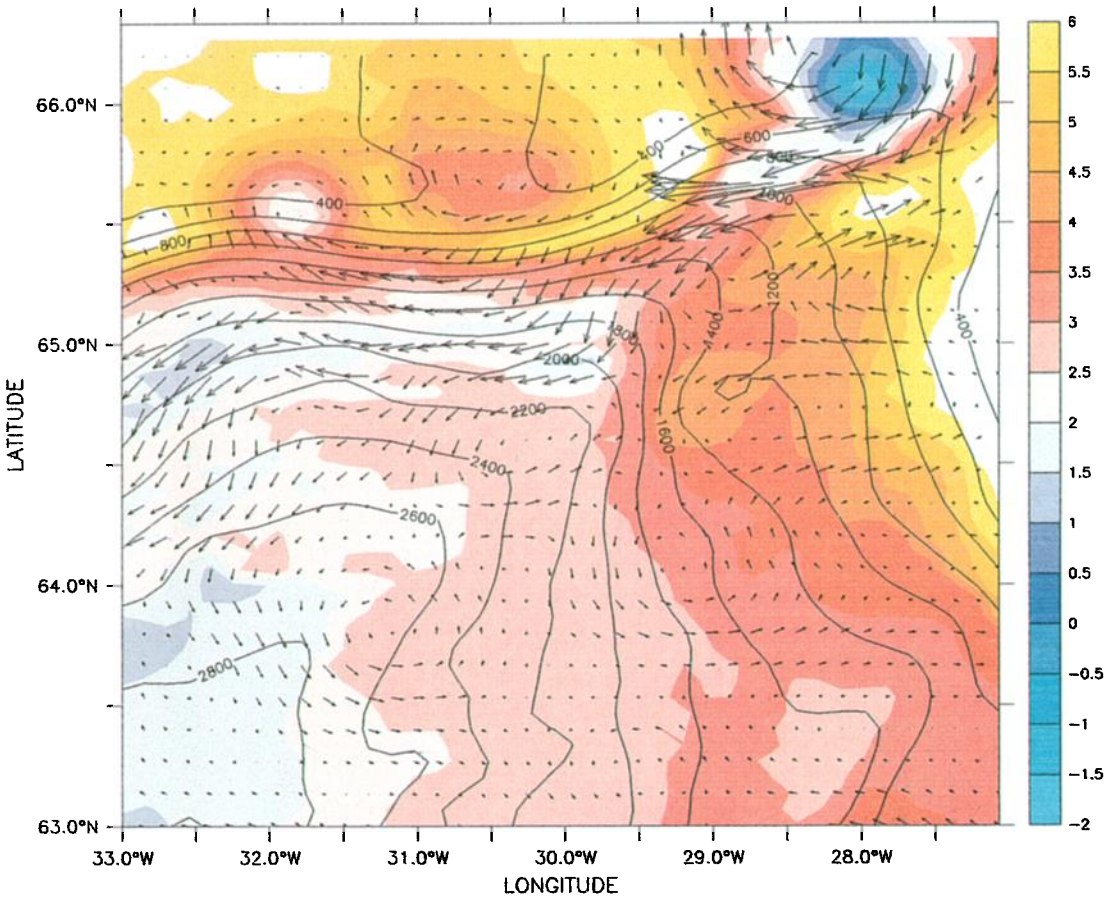

Plate 2. Bottom temperature and overlaid barotropic current vectors from bottom torque equation applied to Poseidon-222/230 conductivity-temperature-depth data set. Note the anticyclonic eddies on the shelf-slope transition region in the north and the cyclones at greater depths in the south.

depths at 66°N, 27.5°W to 2200 m at 65°N, 30.5°W. As in the simulation, the new overflow water is trapped in anticyclones at the upslope regions and there are cyclones at the downslope regions. The descending plume flows between the eddies. The barotropic current vectors overlaid in Plate 2 were calculated from potential energy using a stationary bottom torque equation $B_T = \nabla E \times \nabla H^{-1} = \nabla\psi \times \nabla(fH^{-1})$, where ψ is the barotropic mass transport, H is water depth and $E = \int_{-H}^{0} gz\frac{\rho(z)}{\rho_0}dz$ is the total potential energy [*Marotzke and Willebrand,* 1996]. The computations neglect the bottom friction, but in reality the strong cross-slope sinking requires larger effective bottom friction as in model run RCH. In the model we used a linear drag law. With bottom speeds of typically $0.5\,\mathrm{m\,s^{-1}}$ an equivalent quadratic law would require a drag coefficient of $c_d = r_d < u >^{-1} = 8.3 \times 10^{-4}$ and might be more appropriate in some cases.

The barotropic transport on a section along 65.4°N results in 4 Sv using the bottom torque calculations. Note, however, that the bottom torque equation is strictly valid only for stationary conditions and vanishing nonlinear terms. These conditions are not met in the presence of the strong eddies. On the other hand, the barotropic flow also includes contributions from upper layer processes and the location is south of the control point where entrainment has enlarged the transport. Nevertheless, the order of magnitude is in the range predicted by the model calculations. The model provides a good test to compare the barotropic currents from the torque equation and the exact model velocity (Figure 12). Shown is the vertical integral of the v component on a section at $y = 400$ km of RWL. The core of the overflow is clearly showing up in both curves. The real velocity, however, is larger at the periphery. The bottom torque rule fails there, because the mean flow arises from continuous passage of transient eddies that are not represented by the steady torque equation.

The presence of strong barotropic eddies has previously been noted by *Bruce* [1995] and *Krauss* [1996]. The existence of anticyclones in the Denmark Strait

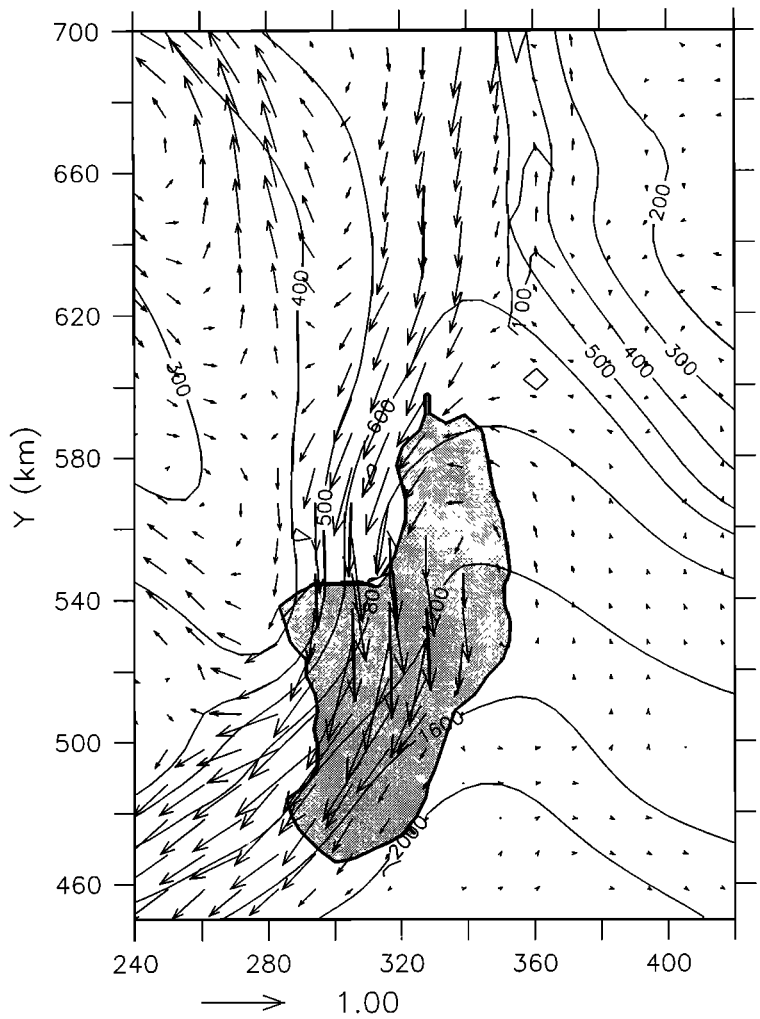

Figure 10. April-to-July average of bottom velocity and critical Froude number $Fr = 1$ contour.

overflow was first mentioned by *Krauss and Käse* [1998] and is a theoretical prediction from reduced gravity models that account for ageostrophic instability mechanisms [*Griffiths et al.*, 1982].

The Poseidon data are not finally processed. The direct transport estimates from combined density and acoustic Doppler current profiler (ADCP) velocity data are therefore not yet available for a detailed comparison with modeling. On a later 1998 Poseidon cruise *T.B. Sanford* from the University of Washington has conducted a detailed survey with expendable velocity probes that directly resolve the bottom boundary layer. This data set has the potential for a systematic description and quantification of the velocity structure in the bottom boundary layer.

5. Discussion

The quantification of the flow of cold and dense water through Denmark Strait is a key problem for climate prediction models. The large-scale ocean circulation models have difficulties in describing the water mass transformations taking place while the plume spills into the Irminger Sea and gradually sinks to greater depths along its path on the East Greenland continental slope. We have applied a process model in bottom following coordinates [*Song and Haidvogel*, 1994] to demonstrate that a suited model and sufficient resolution can address the dynamical behavior of the outflowing plume in compatibility with observations.

Given that the Rossby radius is resolved, the rotating hydraulics can be described properly and the flow behaves as predicted by Whitehead-Killworth maximal flow restrictions developed for idealized configurations.

After these flow limitations have been demonstrated for idealized cases, we applied the model to a fairly realistic topography of the Denmark Strait. The process simulations showed that with a density contrast comparable to the situation in nature, the flow through Denmark Strait has a characteristic value of 2.5 Sv for an interface height above the sill of about 380 m. This is comparable to measurements. Note, however, that due to the smoothed topography the sill depth in the model is 580 m rather than 630 m in reality. Obviously, the transport is strongly modulated by an eddy field generated at the sill exit. It is remarkable that over periods

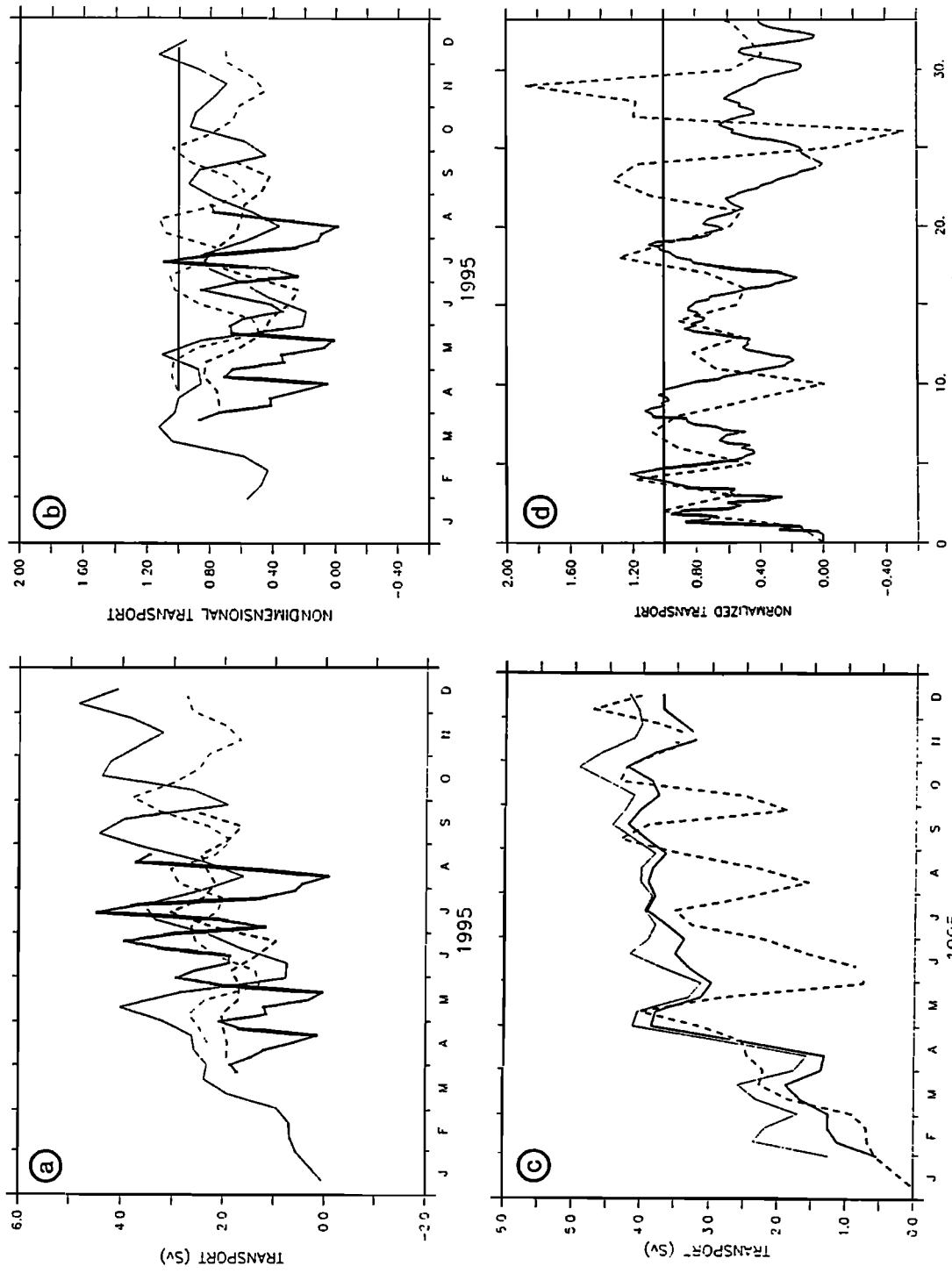

Figure 11. (a) Time development of transport colder than 4.5°C through the sill for the four experiments RWL (thin solid), RWH (thin dashed), RCL (thick solid), and RCH (thick dashed). (b) Transport as in Figure 11a, but scaled by the *Killworth and McDonald* [1993] relation (8). (c) Simulated sill transport of experiment RWL (dashed), computed as suggested by *Whitehead* [1998] using the point $x = 340$ km, $y = 700$ km (thick solid), and the corresponding maximum transport for the *Killworth and McDonald* [1993] relation evaluated at the same location (thin solid). (d) Normalized transport evolution for two dam-break experiments with parameters corresponding to experiments RCL (dashed) and RCH (solid). Note the different time axis compared to Figures 11a to 11c.

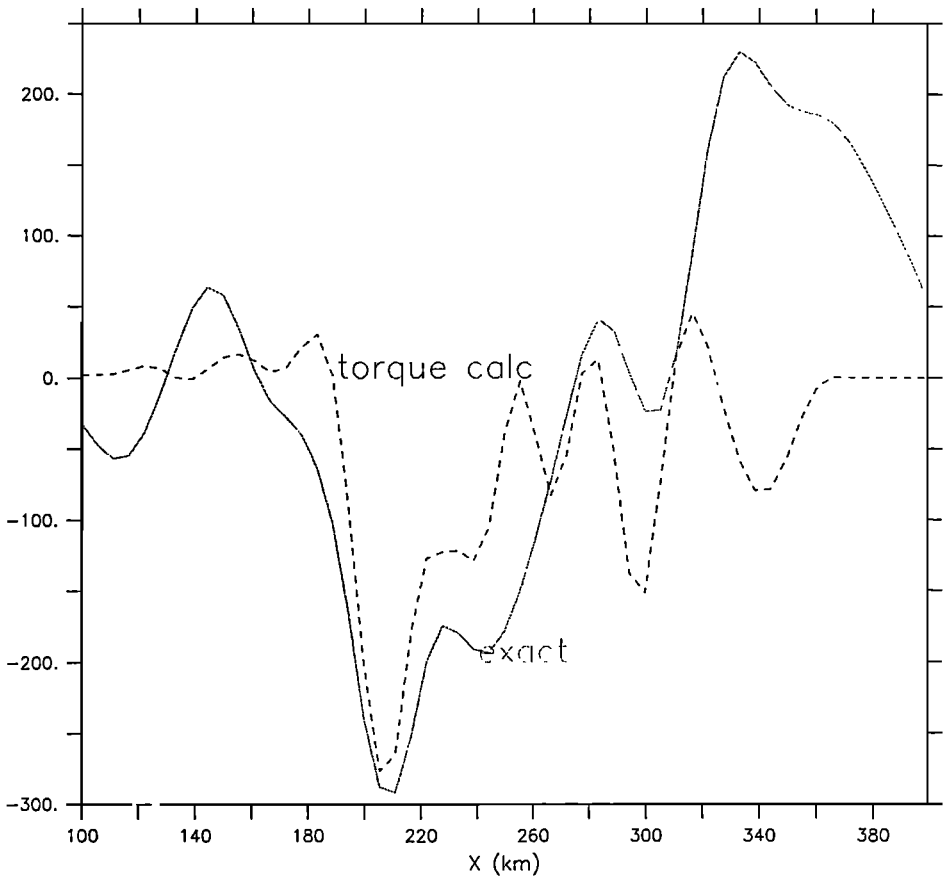

Figure 12. April-July time average on a section normal to the slope at $y = 400$ km of the modeled v component and the estimate from the bottom-torque relation (see text).

of a few days the outflow can cease completely. The reason for this is the formation of a geostrophic front on the Greenland Sea side of the sill, along which an anticyclonic counterflow is developing. The source water contained in this anticyclone detaches periodically with a cyclonic counterpart into the Irminger Sea. While the anticyclones remain near the shallower upslope parts, the cyclones draw water out the frontal region between the two eddies and move into the deeper regions of the Irminger Sea.

The maximum flow depends only weakly on the density of the overflow water. We have shown that increasing the temperature of the inflow by 1°C has negligible effects on the transport. In contrast to this, the plume temperature is raised by the amount prescribed. An active topographic control mechanism thus would buffer transport fluctuations, while communicating quickly the density variation.

Topographic control thus suggests that variations in heat transport are mainly caused by temperature fluctuations while volume transports remain constant. There is some controversy in the interpretation of observations. *Dickson et al.* [1999] argue that increasing temperature in the overflow immediately leads to an upslope shift of the plume core. This is not confirmed by our simulations. The runs with warm and cold inflow have essentially the same location of the mean plume depth. Figure 13 shows a mean temperature section at $y = 300$ km for the warm and cold runs (top panel). It is clearly seen that the core location is unchanged, a consequence of the strong topographical steering and the fact that the eddies are mainly barotropic. To demonstrate the effect of bottom friction, we have changed r_d for the warm run to the high value during the integration. Within only 10 days the warmed core has shifted 30 km downslope and sinks by more than 700 m. The controlling factor for the downstream plume location is thus net bottom drag as well as the size of the eddies.

The overflow is considered a major contributor to the thermohaline overturning. The unsettled question is which amount of water that spills into the Irminger Sea recirculates as a consequence of the hydraulic exchange. In the process model it is easy to identify. For the realistic cases considered we defined the "cold" water by the 4.5°C isotherm, because the return flow occurs above this isotherm depth. On the other hand, we have calculated the heat transport directly and plot it versus the "cold" transport (Figure 14). There is a clear linear relationship with a slope of 0.11 PW per 10 Sv transport. The case with the larger temperature contrast

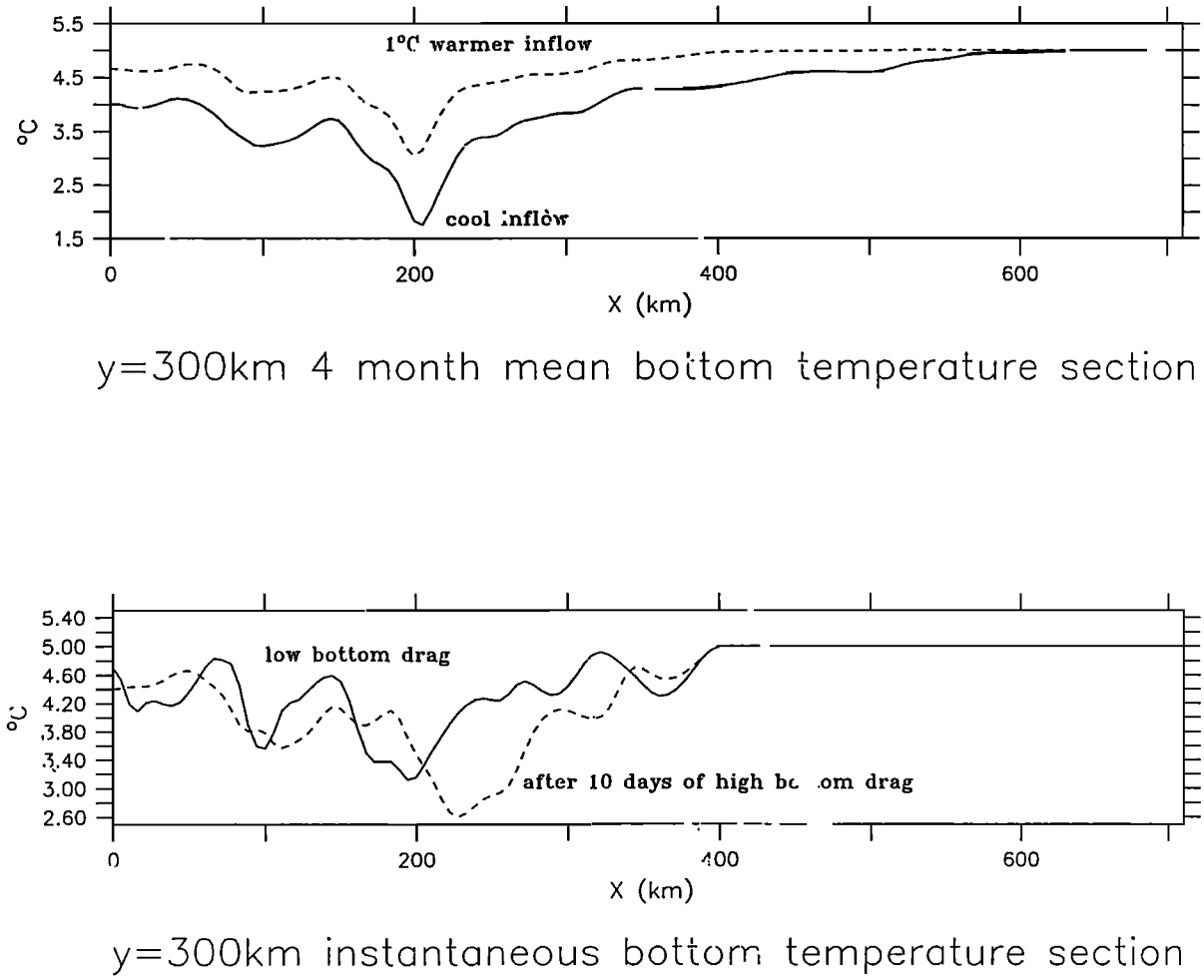

Figure 13. (top) Five month mean bottom temperature on a section normal to the slope 350 km downstream of the sill for run RCL and run RWL. The core of the plume is virtually at the same geographical location and depth. (bottom) Instantaneous snapshot of temperature at the same location at the end of the averaging period of run RWL (full line) and after 10 days of further integration with high bottom drag.

has 0.031 ± 0.024 PW compared to 0.023 ± 0.018 PW for the 1°C warmer inflow case. The eddies are responsible for the scatter in the data, and longer series have to be analyzed for better statistical significance. The trend, on the other hand, is consistent with the findings of the idealized geometry runs. If we define a mean temperature difference between outflowing and inflowing water as δT, then the average temperature of the outflow at 2.5 Sv would be δT=3.1°C for the cool case and 2.3°C for the warm case, respectively. This would be roughly the mixed temperature of donator and receiver, indicating the return flow of mixed water that is larger than assumed by the 4.5°C isotherm choice. Further exploration in models of the interface height would help in the design of observational programs. A successful attempt to measure the heat content in the overflow plume by inverted echo sounders was reported by *Dickson et al.* [1999].

The absolute value of the heat transport by the overflow seems to be rather small, but can be explained easily. The heat loss poleward of the Greenland-Iceland-Scotland ridges amounts to about 0.3-0.4 PW [*Gulev and Tikchonov,* 1989]. The temperature difference of the North Atlantic waters to the East Greenland Current temperatures is about 8°C averaged over the upper layers. A transport of about 10 Sv would result in a 0.3 PW heat transport, which can balance the heat loss alone. Perhaps this is the reason that coarse resolution global climate models really do not need the overflow process for heat balances. The overflow effects therefore may be seen in different areas. The downstream mixing by the overflow eddy chains and instabilities of the deep western boundary current increase the entrainment and therefore spin up the subpolar circulation. Changing temperatures alter the entrainment and cause fluctuations in the cyclonic gyre circulation.

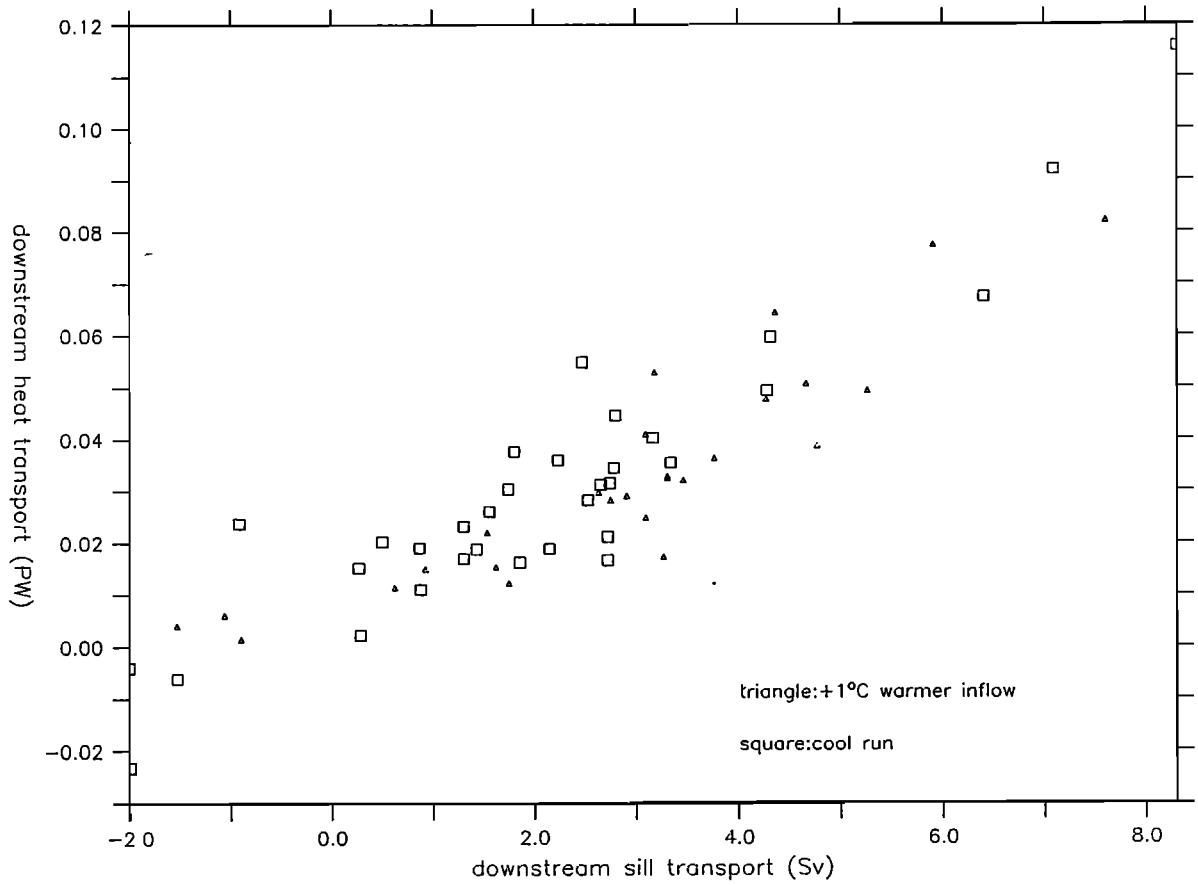

Figure 14. Correlation between cold transport (temperature colder than 4.5°C) and directly calculated heat transport through the sill for runs RCL and RWL.

These changes severely affect the subpolar/subtropical interactions and the heat exchange in these latitudes. The upcoming improved circulation models which resolve the overflow dynamics correctly will contribute strongly to our understanding of the thermaline circulation fluctuations.

Acknowledgments. This work was supported by the Deutsche Forschungsgemeinschaft within the framework of the Sonderforschungsbereich SFB-460-TP-A1.

References

Armi, L., The hydraulics of two flowing layers with different densities, *J. Fluid Mech., 163*, 27–58, 1986.

Bruce, J. G., Eddies southwest of the Denmark Strait, *Deep Sea Res. I, 42*, 13–29, 1995.

Dickson, B., J. Meincke, I. Vassie, J. Jungclaus, and S. Osterhus, Possible predictability in overflow from the Denmark Strait, *Nature, 397*, 243–246, 1999.

Dickson, R. R., and J. Brown, The production of North Atlantic Deep Water: Sources, rates and pathways, *J. Geophys. Res., 99*, 12,319–12,341, 1994.

Ganopolski, A., S. Rahmstorf, V. Petoukhov, and M. Clausen, Simulation of modern and glacial climates with a coupled global model of intermediate complexity, *Nature, 391*, 351–356, 1998.

Griffiths, R. W., P. D. Killworth, and M. E. Stern, Ageostrophic instability of ocean currents, *J. Fluid Mech., 117*, 343–377, 1982.

Gulev, S. K., and V. A. Tikchonov, Interannual variations of the ocean heat balance and meridional heat transport, *Atmos. Ocean Space, 7*, 332–341, 1989.

Jungclaus, J. H., and J. O. Backhaus, Application of a transient reduced gravity plume model to the Denmark Strait Overflow, *J. Geophys. Res., 99*, 12,375–12,396, 1994.

Killworth, P. D., On hydraulic control in a stratified fluid, *J. Fluid Mech., 237*, 605–626, 1992a.

Killworth, P. D., Flow properties in rotating, stratified hydraulics, *J. Phys. Oceanogr., 22*, 997–1017, 1992b.

Killworth, P. D., On reduced-gravity flow through sills, *Geophys. Astrophys. Fluid Dyn., 75*, 91–106, 1994.

Killworth, P. D., Hydraulic control and maximal flow in rotating stratified hydraulics, *Deep Sea Res. I, 42*, 859–871, 1995.

Killworth, P. D., and N. R. McDonald, Maximal reduced-gravity flux in rotating hydraulics, *Geophys. Astrophys. Fluid Dyn., 70*, 31–40, 1993.

Krauss, W., A note on overflow eddies, *Deep Sea Res. I, 43*, 1661–1667, 1996.

Krauss, W., and R. H. Käse, Eddy formation in the Denmark Strait overflow, *J. Geophys. Res., 103*, 15,525–15,538, 1998.

Marotzke, J., and J. Willebrand, The North Atlantic mean circulation: Combining data and dynamics, in *The*

Warmwatersphere of the North Atlantic Ocean, edited by W Krauss, pp. 55–90, Gebr. Bornträger, Berlin, 1996

Mellor, G. L , and T. Yamada, Development of a turbulence closure model for geophysical fluid problems, *Rev. Geophys. Space Phys.*, *20*, 851–875, 1982

Nof, D., The translation of isolated cold eddies on a sloping bottom, *Deep Sea Res. A*, *30*, 171–182, 1983.

Pacanowski, R., C., and S. G. H. Philander, Parameterization of vertical mixing in numerical models of tropical oceans, *J. Phys. Oceanogr.*, *11*, 1443–1451, 1981.

Pratt, L. J., Hydraulic control of sill flow with bottom topography, *J. Phys. Oceanogr.*, *18*, 1970–1980, 1986.

Pratt, L. J., Hydraulically drained flow in rotating basins, II, Steady flow, *J. Phys. Oceanogr.*, *27*, 2522–2535, 1997.

Pratt, L. J., and S. G. Llewellyen Smith, Hydraulically drained flow in rotating basins, I, Method, *J. Phys. Oceanogr.*, *27*, 2509–2521, 1997.

Song, Y., and D. Haidvogel, A semi-implicit ocean circulation model using a generalized topography-following coordinate system, *J. Comput. Phys.*, *115*, 228–244, 1994.

Wadley, M. R., and G. R. Bigg, Interbasin exchange of bottom water in ocean general circulation models, *J. Phys. Oceanogr.*, *24*, 2209–2214, 1994.

Whitehead, J. A., Internal hydraulic control in rotating fluids: Applications to oceans, *Geophys. Astrophys. Fluid Dyn.*, *36*, 187–205, 1989.

Whitehead, J. A., Topographic control of oceanic flows in deep passages and straits, *Rev. Geophys.*, *36*, 423–440, 1998.

Willebrand, J., B. Barnier, C. Böning, C. Dieterich, P. Herrmann, P. D. Killworth, C. LeProvost, Y. Jia, J.-M. Molines and A. L. New, Circulation characteristics in three eddy-permitting models of the North Atlantic, *Progr. Oceanogr.* in press, 2000.

Rolf H. Käse and Andreas Oschlies, Institut für Meereskunde an der Universität Kiel, Düsternbrooker Weg 20, 24105 Kiel, Germany. (rkaese@ifm.uni-kiel.de; aoschlies@ifm.uni-kiel.de)

(Received May 4, 1999; revised February 25, 2000; accepted April 18, 2000.)